ORIGINAL PAPER

Evaluation of a Polyethylene Glycol Phantom for Measuring Apparent Diffusion Coefficients Using Three 3.0 T MRI Systems

Eisuke Sato[1] · Kei Fukuzawa[2] · Hiroyuki Takashima[3] · Yuya Yamatani[4] ·
Yasuo Takatsu[5] · Junichi Hata[6] · Keigo Hikishima[7] · Kenta Miwa[8]

Abstract

We aimed to examine the possibility that polyethylene glycol (PEG) phantoms can simulate apparent diffusion coefficients (ADCs) of malignant tumors and the effectiveness of PEG phantoms using three 3.0 T magnetic resonance imaging (MRI) systems. In particular, the correlations between PEG concentrations and ADC values, the validation of ADC measurement precision, and the stability and reproducibility of PEG phantom were verified. A phantom containing 0, 0.625, 1.250, 2.5, 5, 10, 20 mM PEG was assessed using three MRI systems. The endpoints comprised correlations between PEG concentrations and ADC, validation of ADC measurement precision and the stability and reproducibility of the PEG phantom. The correlation coefficients between PEG concentrations and the ADC of the three MRI systems and among the three MRI systems revealed negative ($r \approx -1.000$, $P < 0.001$) and positive ($r \approx 1.000$, $P < 0.001$) correlations. The ADC_{mean} of 2.5–20 mM PEG was significant ($P < 0.05$ t tests), and that at ≥ 10 mM PEG was $< 1.0 \times 10^{-3}$ mm²/s. The %CV ranged from 1.20 to 4.62, and repeatability was confirmed by the 90% confidence interval. The maximum values for $Difference_{Change\ over\ time}$ and $Difference_{Pri.vs.New}$ were 0.20 and 0.19×10^{-3} mm²/s, respectively. In this study, we found that PEG concentrations ≥ 10 mM are required to simulate the ADCs of malignant tumors ($ADC < 1.0 \times 10^{-3}$ mm²/s). We also showed that the ADC value is easily controlled by adjusting PEG concentrations, and can be stably measured using our PEG phantom for at least 6 months. The PEG phantom can easily and stably simulate the ADC of malignant tumors with high reproducibility.

✉ Eisuke Sato
e.sato.ft@juntendo.ac.jp

Extended author information available on the last page of the article

1 Introduction

Diffusion weighted imaging (DWI) is sensitive to water motion, and is, therefore, an important form of imaging in magnetic resonance imaging (MRI), because it provides quantitative values [1]. Moreover, DWI has been widely used in clinical practice to detect early cerebral ischemia [2], detect tumors in the whole body [3], and visualize brain white matter [4]. Also, the apparent diffusion coefficient (ADC) is used to differentiate or determine the effects of treatments on oncogenic lesions and contributes considerably to qualitative diagnoses [5–7]. The ADC is a quantitative index in DWI that can differentiate malignant from benign tumors. For example, the reported threshold ADC that can distinguish a benign mass from malignant breast cancer is $0.95 \pm 0.10 \times 10^{-3}$ mm^2/s [8]. Some malignant tumors show an ADC of less than 1.0×10^{-3} mm^2/s. Therefore, it is important to quantify the ADC of malignant tumors for oncological purposes. The ADC is obviously clinically useful, but it is influenced by various factors including scan parameters, slew rates, pulse sequence design, magnetic field, and the MRI system, causing variances in the ADC even when the same object is repeatedly measured. A study of the relationship between scan parameters and ADC has found that a long TR and a short TE are effective for precise ADC measurements [9]. Even when scan parameters are fixed, differences among MRI scanners slightly influence the ADC [10]. In fact, the ADC of 12 healthy volunteers measured using 10 MRI systems significantly differed [11]. One study of seven healthy volunteers found significant inter-scanner differences in the ADC of gray matter [12]. These findings indicated that the quantifiability and reproducibility of ADC measurements requires improvement by determining the dependence of these factors before starting measurements. However, individual differences might affect the results of imaging humans. Therefore, a constant standard ADC evaluation phantom is needed.

The motion of water molecules in living tissue includes not only free diffusion but also restricted diffusion due to several factors (e.g., internal physiological perfusion, cell membrane structure, and other tissue compartments). Therefore, a standard phantom to investigate the precision of ADC measurement requires restricted diffusion. There have been several published reports on phantoms for evaluating ADCs. Among them, the ice-water phantom [13, 14] has the ADC values of approximately 1.1×10^{-3} mm^2/s and has been reported to be useful as the ADC evaluation phantom. Also, the Quantitative Imaging Biomarkers Alliance (QIBA)/National Institutes of Health (NIH)/NIST isotropic diffusion phantom [15] has been reported to be useful as a reference phantom that can evaluate the repeatability and reproducibility of ADC values [16, 17]. In a multi-center study conducted with ice-water phantom [13], the standardization of the DWI protocol improved the reproducibility of ADC measurements and reported that the source of error in multi-center studies was spatial ADC non-uniformity. Also, the QIBA profile provides small inter-system, inter-site, and temporal variations that allow for quantitative evaluation. For the above reasons, the use of the QIBA/NIH/NIST isotropic diffusion phantom and measurement according to the QIBA

profile is recommended for the quantitative evaluation of ADC values in multi-center studies. The ice-water phantom or the QIBA/NIH/NIST isotropic diffusion phantom, a quality assurance tool for precise ADC measurements, refers to the commissioning of the MRI machine and fitting the algorithm at 0 °C. However, the correct ADC measurements at 0 °C do not imply correct room temperature or tissue in vivo ADC measurements. On the other hand, PEG has the advantage of changing the ADC values by adjusting the PEG concentrations, although we need to observe to the temperature more, as reported in a previous study [18]. Sucrose solutions [1, 19, 20] and PAG (Polyacrylamide) phantom [21] have also the advantage of changing the ADC by adjusting the concentration when fabricating the phantom. Controlling ADC with their concentration suggests the possibility of simulating ADC of malignant tumors (ADC $< 1.0 \times 10^{-3}$ mm^2/s). The main advantage of PEG is that they are ready to use, commercially available, without the need of in-house fabrication process. Furthermore, the PEG is inexpensive and thus affordable for any institution.

We aimed to examine the possibility that PEG phantoms can simulate ADCs of malignant tumors and the effectiveness of PEG phantoms using three 3.0 T MRI systems. In particular, the correlations between PEG concentrations and ADC values, the validation of ADC measurement precision, and the stability and reproducibility of PEG phantom were verified.

2 Materials and Methods

2.1 Preparation of PEG Phantom

Figure 1 shows a schematic view of the PEG phantom. The PEG (MP Biomedicals Inc., Santa Ana, CA, USA) used herein has a molecular weight of 8000. Plastic vials (45×80 mm) containing 0-, 0.625-, 1.25-, 2.5-, 5-, 10- and 20-mM PEG were placed in a 170×110 mm plastic container and fixed using agarose (FUJIFILM Wako Pure Chemical Corp., Osaka, Japan) dissolved in Milli-Q water to form a gel. The 0 mM indicates PEG-free water only.

2.2 ADC Measured Using PEG Phantom

The ADC was measured using the PEG phantom with MAGNETOM Verio (Siemens Healthcare, Erlangen, Germany), Signa HDxt (GE Healthcare, Waukesha, WI, USA) and Ingenia (Philips Healthcare, Best, The Netherlands) 3.0-T MRI systems (Table 1). We defined the MAGNETOM Verio (Siemens Healthcare) as Scanner A, Signa HDxt (GE Healthcare) as Scanner B, and Ingenia (Philips Healthcare) as Scanner C. The surface temperature of the PEG phantom was fixed at 22.0 °C by placing it in the center of a head coil for several hours, and maintained at 22.0 °C during image acquisition. Table 2 shows the DWI scan parameters of the three MRI systems that are normally used for acquiring clinical images of the head. Therefore, we set the b-factor to 1000 s/mm^2. The scan parameters, such as field of view (FOV) and echo time (TE), were
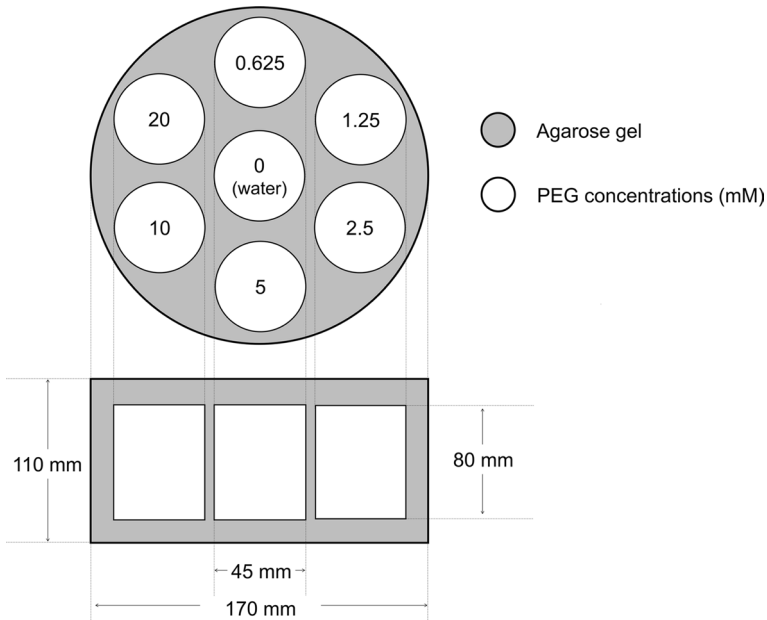
Fig. 1 Schematic view of PEG phantom. Vials containing 0, 0.625, 1.250, 2.5, 5, 10, 20 mM PEG are immobilized in agarose gel within a plastic container. Vial containing 0 mM PEG (water) is centered in phantom. Above that is vial containing 0.625 mM PEG, then vials containing 1.25–20 mM PEG are arranged clockwise around center vial

Table 1 Characteristics of 3.0 T MRI systems

MR system	Scanner A	Scanner B	Scanner C
Coil (channels)	32	8	16
Parallel imaging	Yes	Yes	Yes
Sensitivity correction	Yes	Yes	Yes
Slew rate (T/m/s)	200	150	200

modified to consider the effects of DWI distortion. In each MRI system, the TE was selected to be the shortest when b factor $= 1000$ s/mm^2. The slice position of the DWI was set to the isocenter that was the center of the PEG vial. Regions of interest (ROI) were set to acquire the signal intensity from the DWI of each PEG (0–20 mM) using in-house software of the three MRI systems (Scanner A, B, and C). The determined ROI shape was circular and the ROI size was $> 70\%$ (> 816 mm^2) of the area of the PEG vial. The mean ADC of five scans at each PEG concentration were calculated using Eq. (1) [11] built in Microsoft® Excel®, where b_0 is 0 s/mm^2, b_1 is 1000 s/mm^2, $\mathrm{SI}(b_0)$ is the signal intensity at $b=0$ s/mm^2, and $\mathrm{SI}(b_1)$ is the signal intensity at $b=1000$ s/mm^2.

$$\mathrm{ADC}\left[\mathrm{mm}^2/\mathrm{s}\right] = \ln\left[\mathrm{SI}(b_1)/\mathrm{SI}(b_0)\right]/(b_1 - b_0). \tag{1}$$

Table 2 Scan parameters of DWI using 3.0 T MRI systems

MR system	Scanner A	Scanner B	Scanner C
TR (ms)	10,000	10,000	10,000
TE (ms)	74	79	86
FOV (mm)	400×250	250×250	250×250
Acquired matrix (reconstructed matrix)	128×78 (256×156)	128×128 (256×256)	128×128 (256×256)
Number of slices	1	1	1
Slice thickness (mm)	5	5	5
Number of signals averaged	3	3	3
Reduction factor	3	2	4
b-factor (s/mm^2)	1000	1000	1000
Receiver bandwidth (Hz/pixel)	2604	3906	2860
Fat-suppression	CHESS	SSRF	SPIR

CHESS chemical shift selective, *SSRF* spatial-spectral radio frequency, *SPIR* spectral inversion recovery

Correlations between PEG concentrations and ADC, and among the three MRI systems at each PEG concentration were statistically evaluated using Pearson correlation analysis by SPSS version 20.0 (IBM Corp., Armonk, NY, USA). Values with $P < 0.001$ were taken as being significantly different. The mean ADC (ADC$_{mean}$) was calculated from the ADC measured by each of the MRI systems. An ADC$_{mean}$ of 0 mM was defined as the control, and those of the other PEG concentrations were statistically analyzed using *t* tests, with $P < 0.05$ indicating a significant difference. In addition, the linear equation and correlation coefficient between PEG concentration and ADC value were determined for each MRI system.

2.3 Validation of ADC Measurement Precision

Measurement errors in ADC evaluation are important to understand. To verify the setting errors of PEG phantoms by operators, we re-set the PEG phantoms at each of five image acquisitions. Analytical errors in ROI settings were verified over five repeated ROI analyses of each image. The surface temperature of the PEG phantom was fixed at 22.0 °C by placing it in the center of a head coil for several hours, and maintained at 22.0 °C during image acquisition. The scan parameters and ROI settings for the acquisition of these data were the same as in those described above. The mean $\pm$ standard deviation (SD) of the ADC at each PEG concentration was determined, then, the coefficient of variation (%CV) was calculated from these values as follows:

$$\% \, CV = \frac{Mean}{SD} \times 100. \tag{2}$$

2.4 Change Over TIME and Reproducibility of PEG Phantom

Images were acquired from the primary PEG phantom (P0) prepared as described in the Methods subsection entitled, "Preparation of PEG Phantoms" using scanner C at 3 months later (P3) and 6 months later (P6) to study changes in the PEG phantom over time. Six months after the primary phantom (P0) was created, we also similarly created another PEG phantom (NP6). We verified the reproducibility of this PEG phantom by comparing the ADC with that of P0. The scan parameters, ROI settings, and ADC measurement methods for acquiring these data were the same as in the subsection, "ADC measured using PEG phantom". The surface temperature of the PEG phantom was fixed at 22.0 °C by placing it in the center of a head coil for several hours, and maintained at 22.0 °C during image acquisition. The ADC at month 0 served as the control. Differences in ADC over time within the primary PEG phantom (Difference$_{\text{Change over time}}$) and between the primary and the new phantom (Difference$_{\text{Pri. vs. New.}}$) were calculated using Eqs. (3.1), (3.2), (4.1), and (4.2), respectively:

$$\text{Difference}_{\text{change over time}} = \text{ADC}_{\text{Pri.month0}} - \text{ADC}_{\text{Pri.months3or6}} \tag{3.1}$$

$$\text{Difference}_{\text{changeovertime}}[\%] = \left(\frac{\text{ADC}_{\text{Pri.month0}} - \text{ADC}_{\text{Pri.months 3 or 6}}}{\text{ADC}_{\text{Pri.month 0}}} \right) \times 100 \tag{3.2}$$

$$\text{Difference}_{\text{Pri. vs New.}} = \text{ADC}_{\text{Pri. month 0}} - \text{ADC}_{\text{New. month 6}} \tag{4.1}$$

$$\text{Difference}_{\text{Pri. vs New.}}[\%] = \left(\frac{\text{ADC}_{\text{Pri. month 0}} - \text{ADC}_{\text{New month 6}}}{\text{ADC}_{\text{Pri. month 0}}} \right) \times 100. \tag{4.2}$$

3 Results

3.1 Correlations Between PEG Concentrations and ADC

Figure 2 shows correlations between PEG concentrations and ADC determined by the three MRI systems. The ADC decreased as PEG concentrations increased according to all three systems. The correlation coefficients (r) between PEG concentrations and the ADC of all three MRI systems revealed a high negative correlation (Scanner A; $r = -0.949$, Scanner B; $r = -0.939$, Scanner C; $r = -0.961$), with $P < 0.001$ vs. 0 mM PEG. The correlation coefficients (r) among the three MRI systems revealed a close positive correlation (Scanner B; $r = 0.996$, Scanner C; $r = 0.997$), with $P < 0.001$ vs. Scanner A.

Figure 3 shows the means $\pm$ SD of the mean ADC (ADC$_{\text{mean}}$) values determined from the three MRI systems. The ADC$_{\text{mean}}$ at 0, 0.625, 1.25, 2.5, 5, 10 and 20 mM were $2.08 \pm 0.12 \times 10^{-3}$, $2.03 \pm 0.14 \times 10^{-3}$, $1.93 \pm 0.14 \times 10^{-3}$, $1.77 \pm 0.06 \times 10^{-3}$,
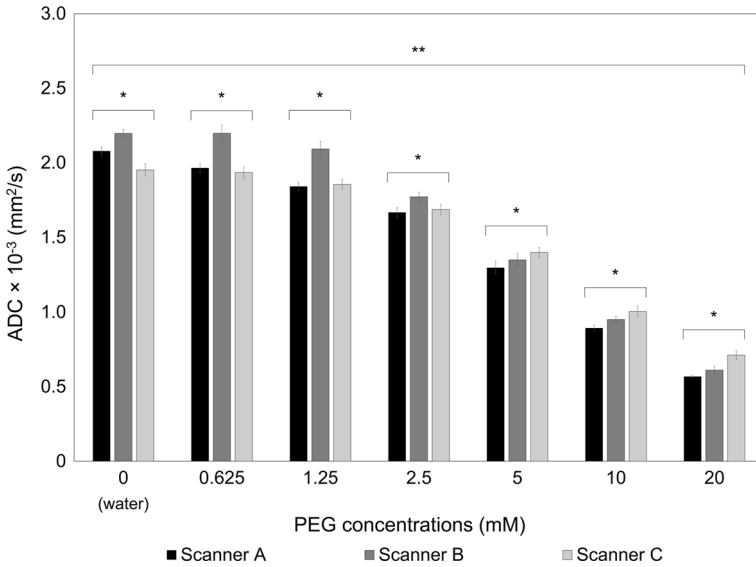
Fig. 2 Correlations between PEG concentrations and ADC determined using three MRI systems. Data are presented as means $\pm$ SD. Graph shows decreasing ADC with increasing PEG concentrations. Correlation coefficients (r) between PEG concentrations and ADC of three MRI systems show high negative correlation ($r \approx -1.000$, **$P < 0.001$; Pearson correlation analysis) and those among three MRI systems show high positive correlation ($r \approx 1.000$, *$P < 0.001$, Pearson correlation analysis). *ADC* apparent diffusion coefficients, *MRI* magnetic resonance imaging, *PEG* polyethylene glycol
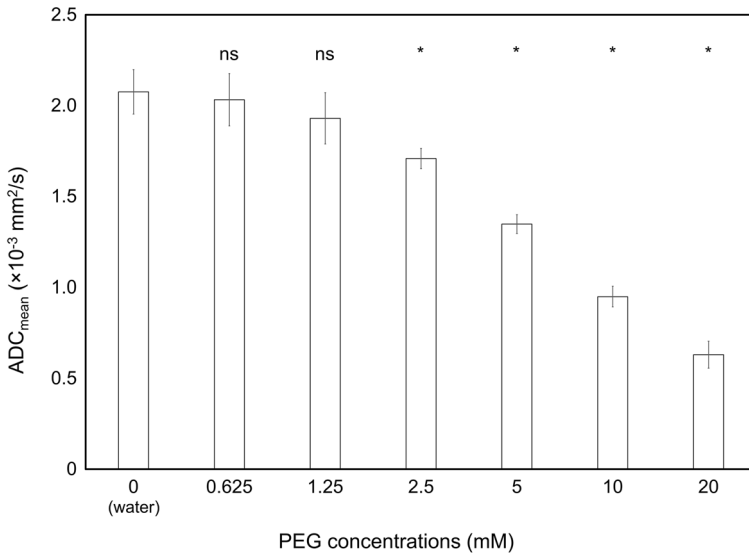
Fig. 3 ADC_{mean} determined from three MRI systems. Data are presented as means $\pm$ SD. *$P < 0.05$ versus 0 mM PEG (t tests). *ADC* apparent diffusion coefficients, *PEG* polyethylene glycol

$1.35 \pm 0.05 \times 10^{-3}$ mm^2/s, $0.95 \pm 0.05 \times 10^{-3}$ and $0.63 \pm 0.07 \times 10^{-3}$ mm^2/s, respectively. The ADC$_{mean}$ significantly differed at ≥ 2.5 mM PEG in all three systems ($P < 0.05$, t tests).

The results of the linear equation between PEG concentration and ADC value for each MRI system are as follows: Scanner A is $y = -0.0754x + 1.897$ ($r = 0.949$), Scanner B is $y = -0.0831x + 2.062$ ($r = 0.939$), and Scanner C is $y = -0.0652x + 1.873$ ($r = 0.961$), where y is the ADC values, x is the PEG concentration, and r is the correlation coefficient.

3.2 Validation of ADC Measurement Precision

Table 3 shows that the mean ($\pm$ SD) ADC and %CV of five images acquired using the three MRI systems decreased with increasing PEG concentrations. The ADC ranged from 0.57 ± 0.01 (20 mM, Scanner A) to 2.20 ± 0.03 (0 mM, Scanner B), and the %CV ranged from 1.20 (0 mM, Scanner B) to 4.62 (20 mM, Scanner B).

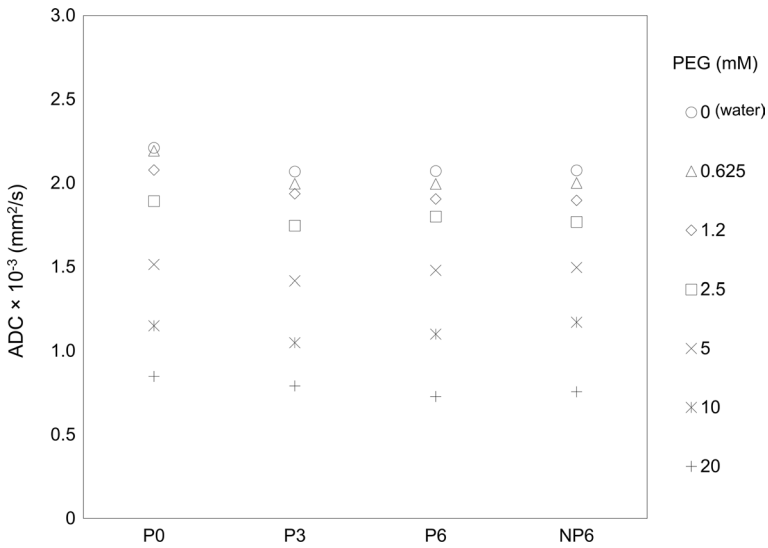## 3.3 Stability and Reproducibility of PEG Phantom

We defined the time when the primary PEG phantom was prepared as month 0 (P0). We then compared the ADC of this phantom at 3 (P3) and 6 (P6) months later and also with the new PEG phantom at month 6 (NP6). Figure 4 and Table 4 show that the stability measured as differences in ADC over time (Difference$_{Change\ over\ time}$) and the reproducibility measured as differences in ADC between the primary and the new phantom (Difference$_{Pri.vs.New}$) ranged from 0.03×10^{-3} to 0.20×10^{-3} mm^2/s (1.60–9.03%), and from -0.02×10^{-3} to 0.19×10^{-3} mm^2/s (-0.95 to 8.19%), respectively.

Table 3 ADC and %CV of three MRI systems

PEG concentrations (mM)	Scanner A		Scanner B		Scanner C	
	Mean $\pm$ SD	%CV	Mean $\pm$ SD	%CV	Mean $\pm$ SD	%CV
0 (water)	2.08 ± 0.03	1.43	2.20 ± 0.03	1.20	1.95 ± 0.04	2.08
0.625	1.96 ± 0.03	1.53	2.19 ± 0.06	2.59	1.93 ± 0.04	1.99
1.25	1.84 ± 0.03	1.54	2.09 ± 0.05	2.37	1.86 ± 0.04	1.84
2.5	1.67 ± 0.04	2.04	1.77 ± 0.03	1.70	1.69 ± 0.04	1.99
5	1.30 ± 0.04	3.25	1.35 ± 0.05	3.15	1.40 ± 0.04	2.35
10	0.89 ± 0.02	2.32	0.95 ± 0.02	2.40	1.00 ± 0.04	3.62
20	0.57 ± 0.01	1.46	0.61 ± 0.03	4.62	0.71 ± 0.03	4.06

ADCs are shown in units of $\times 10^{-3}$ mm^2/s. %CVs are shown in units of ratios (%)

Fig. 4 Comparison of changes in ADC over time (stability) and of phantoms prepared 6 months apart (reproducibility). *ADC* apparent diffusion coefficient, *PEG* polyethylene glycol, *P0, P3, P6* primary phantom at month 0, and at 3 and 6 months thereafter, *NP6* a new PEG phantom prepared at 6 months after primary PEG phantom (month 0; P0)

Table 4 Differences in ADC at various PEG concentrations over time and between primary and new phantoms

PEG concen-trations (mM)	Difference$_{Change\ over\ time}$		Difference$_{Pri.\ vs\ New}$
	P0 vs. P3	P0 vs. P6	P0 vs. NP6
0 (water)	0.14 (6.38%)	0.14 (6.29%)	0.13 (6.06%)
0.625	0.20 (8.91%)	0.20 (9.03%)	0.19 (8.69%)
1.25	0.14 (6.43%)	0.17 (7.89%)	0.18 (8.19%)
2.5	0.15 (6.61%)	0.09 (4.20%)	0.12 (5.61%)
5	0.10 (4.39%)	0.03 (1.60%)	0.02 (0.81%)
10	0.10 (4.57%)	0.05 (2.28%)	− 0.02 (− 0.95%)
20	0.06 (2.58%)	0.12 (5.47%)	0.09 (4.16%)

ADCs are shown in units of $\times 10^{-3}$ mm^2/s. The % indicates the ratio of change in ADCs

4 Discussion

The main idea points of our study are to evaluate the correlation between PEG concentration and ADC, the validation of ADC measurement precision, the changes over time of PEG phantom, and the reproducibility of PEG phantom using three MRI systems under general conditions.

This study evaluated PEG phantom in different MRI systems in terms of PEG concentration, %CV, stability, and reproducibility. Moreover, we concluded that

PEG concentration was determined for the simulation of ADCs of a malignant tumor. Furthermore, the ADC_{mean} significantly differed at ≥ 2.5 mM PEG in all three systems ($P < 0.05$, t tests). Previous studies of ADC measurements have used phantoms containing agarose [22], polyacrylamide [23], nickel-doped agarose/sucrose gels [1], PEG [18, 24], PVP [25, 26] and ice-water [20]. One of these studies [25], obtained ADC ranging from 0.5 to 1.1×10^{-3} mm^2/s by adjusting the PVP concentration between 0 and 25% w/w. Furthermore, ADC decreased as PVP concentrations increased. Similarly, ADC decreased in phantoms containing increasing concentrations of agar gels and sucrose solutions [14]. Others have also found that ADC decreases in phantoms with increasing PEG concentrations [18, 24]. The authors of these reports noted that these phantoms might serve as ADC standard phantoms. Our results were comparable to their findings. That is, PEG concentrations can be adjusted to control ADC. Therefore, the ADC of clinical lesions can be simulated by adjusting PEG concentrations in a phantom. Notably, the ADC is $< 1.0 \times 10^{-3}$ mm^2/s at PEG concentrations ≥ 10 mM, whereas that of malignant tumors is often $\leq 1.0 \times 10^{-3}$ mm^2/s [27]. The novel finding that PEG concentrations can express ADC $\leq 1.0 \times 10^{-3}$ mm^2/s is clinically useful.

In our study, DWI data were obtained by re-setting the phantom on each scan using the clinical scan parameters routinely used in each MR system. A previous multi-center study on DWI examined the imaging position and repeatability of ADCs in each MR system using a standardized protocol [13]. This report shows that the standard deviation of bore center ADCs is less than 2%, day-to-day repeatability is within 4.5%, intra-exam repeatability at the phantom center is within 1%, and inter-site reproducibility of ADC at magnet isocenter should be within 3%, vendor and system-specific spatial non-uniformity ADC bias should be more than 10% off-center. Ogura et al. [10] reported a %CV of ADC for six MRI systems of 3.32%, and a %CV for ten repeated measurements of one individual within 1 day of 1.72%. Our ADC values were obtained from PEG phantoms in three MR systems using a routine scanning protocol in clinical practice. Our results showed an SD of 0.01–0.06 and a %CV of 1.20–4.06%, which are approximately comparable to previous studies [10, 13]. However, our data may include a variety of error factors (e.g., system, operator, analyzer, phantom setting, scan protocol, etc.). Although, these variabilities may not be enough compared to the values of previous studies, we found that our PEG phantom was able to obtain ADC values within %CV of 5%. The stability measured as differences in ADC over time (Difference$_{Change\ over\ time}$) was within 10% and the reproducibility measured as differences in ADC between the primary and the new phantom (Difference$_{Pri.vs.New}$) was within 9%. Based on the results that showed a maximum variation of 6.38% at a PEG concentration of 0 mM (water), we believe that the differences in ADC values may be a factor of measurement error rather than chemical modification of PEG. However, it was shown that the ADC values may be obtained within 10% of the remeasurement within 6 months or when the phantoms were reproduced.

The study limitations are as follows. We maintained the temperature of the PEG phantom simply by placing it in a head coil for several hours. In addition, we carefully verified that the surface temperature of the PEG phantom was fixed at 22.0 °C while acquiring images. Although we did not evaluate temperature

dependence, ADC values might be stably and reproducibly measured by the PEG phantom under conditions of a constant surface temperature. Chenevert et al. described an ice-water phantom with a known diffusion coefficient and noted that ADC are temperature dependent across multiple vendors [14]. Moreover, differences among vendors remained unresolved in that study compared with the present findings. Although the correlation coefficients among the three MRI systems revealed a close positive correlation (Fig. 2), the difference in ADC values at the PEG concentration of 1.25 mM between Scanner A and Scanner B was the maximum (Table 3). We did not compare the PEG phantom with phantoms containing other materials, the influences of scan parameters of the slew rates of the three MRI systems, as this was not the aim of the study. However, the assessment of quantitative values is very important and several methods (1 imaging procedure, 2 + procedures, 3 multiple studies) have been proposed for evaluating quantitative values in multi-centers [28]. In our study, we consider the "1 imaging procedure" is the most important subject of these methods. Sullivan et al. [28] distinguish between "statistical methods based on knowing the true value" and "methods where the reference standard provides a measurement that contains errors". Our approach corresponds to the latter approach (i.e., the methods where the reference standard provides a measurement that contains errors), and we evaluated the bias, repeatability, and reproducibility of ADC measurements using PEG phantoms in this study. On the other hand, we have determined the linearity and correlation of ADC measurements using the PEG phantom with each MRI system, however, we have not yet been able to obtain the true value of ADC with the PEG phantom. Nevertheless, the ADC value of water (0 mM PEG) at 22 °C could be considered as a reference for the true value of the phantom of this study. A phantom for ADC measurement that provides stable and reproducible ADC values is important to verify these influences (e.g., QIBA/NIH/NIST isotropic diffusion phantom). In addition, we believe that the ADC values must be measured according to the QIBA profile. QIBA phantom is an excellent means for precise measurements in ADC values, however these measurements are performed in 0 °C [16]. There is a need to examine also the ADC measurements in higher temperature (room temperate or tissue in vivo), as it is performed with other phantoms too such as PEG, PAG, sucrose, etc. Therefore, the PEG phantom and the other solutions can be used alternatively for ADC measurements.

5 Conclusion

In this study, we found that PEG concentrations ≥ 10 mM are required to simulate the ADCs of malignant tumors (ADC $< 1.0 \times 10^{-3}$ mm^2/s). We also showed that the ADC value is easily controlled by adjusting PEG concentrations, and can be stably measured using our PEG phantom for at least 6 months. The PEG phantom can easily and stably simulate the ADC of malignant tumors with high reproducibility.

References

1. I. Lavdas, K.C. Behan, A. Papadaki, D.W. McRobbie, E.O. Aboagye, J. Magn. Reson. Imaging **38**, 173–179 (2013)
2. M. Bateman, L.A. Slater, T. Leslie-Mazwi, C.Z. Simonsen, S. Stuckey, R.V. Chandra, Top. Magn. Reson. Imaging **26**, 77–82 (2017)
3. A. Stecco, Leuk. Lymphoma **59**, 2546–2556 (2018)
4. Y. Assaf, O. Pasternak, J. Mol. Neurosci. **34**, 51–61 (2008)
5. S. Higano, X. Yun, T. Kumabe, M. Watanabe, S. Mugikura, A. Umetsu, A. Sato, T. Yamada, S. Takahashi, Radiology **241**, 839–846 (2006)
6. K. Kono, Y. Inoue, K. Nakayama, M. Shakudo, M. Morino, K. Ohata, K. Wakasa, R. Yamada, AJNR Am. J. Neuroradiol. **22**, 1081–1088 (2001)
7. Y. Tsushima, A. Takahashi-Taketomi, K. Endo, J. Magn. Reson. Imaging **30**, 249–255 (2009)
8. E. Rubesova, A.S. Grell, V. De Maertelaer, T. Metens, S.L. Chao, M. Lemort, J. Magn. Reson. Imaging **24**, 319–324 (2006)
9. A. Ogura, K. Hayakawa, T. Miyati, F. Maeda, Eur J Radiol. **77**, 185–188 (2011)
10. A. Ogura, T. Tamura, M. Ozaki, T. Doi, K. Fujimoto, T. Miyati, Y. Ito, F. Maeda, H. Tarewaki, M. Takahashi, J. Comput. Assist. Tomogr. **39**, 760–765 (2015)
11. M. Sasaki, K. Yamada, Y. Watanabe, M. Matsui, M. Ida, S. Fujiwara, E.I. Shibata, Acute Stroke Imaging Standardization Group-Japan. Radiology **249**, 624–630 (2008)
12. N. Tsujita, N. Kai, Y. Fujita, Y. Hiai, T. Hirai, M. Kitajima, Y. Yamashita, R. Murakami, Magn. Reson. Med. Sci. **13**, 81–87 (2014)
13. D. Malyarenko, C.J. Galbán, F.J. Londy, C.R. Meyer, T.D. Johnson, A. Rehemtulla, B.D. Ross, T.L. Chenevert, J Magn. Reson. Imaging **37**, 1238–1246 (2013)
14. T.L. Chenevert, C.J. Galbán, M.K. Ivancevic, S.E. Rohrer, F.J. Londy, T.C. Kwee, C.R. Meyer, T.D. Johnson, A. Rehemtulla, B.D. Ross, J. Magn. Reson. Imaging **34**, 983–987 (2011)
15. K.E. Keenan, J.R. Biller, J.G. Delfino, M.A. Boss, M.D. Does, J.L. Evelhoch, M.A. Griswold, J.L. Gunter, R.S. Hinks, S.W. Hoffman, G. Kim, R. Lattanzi, X. Li, L. Marinelli, G.J. Metzger, P. Mukherjee, R.J. Nordstrom, A.P. Peskin, E. Perez, S.E. Russek, B. Sahiner, N. Serkova, A. Shukla-Dave, M. Steckner, K.F. Stupic, L.J. Wilmes, H.H. Wu, H. Zhang, E.F. Jackson, D.C. Sullivan, J. Magn. Reson. Imaging **49**, e26–e39 (2019)
16. E.M. Palacios, A.J. Martin, M.A. Boss, F. Ezekiel, Y.S. Chang, E.L. Yuh, M.J. Vassar, D.M. Schnyer, C.L. MacDonald, K.L. Crawford, A. Irimia, A.W. Toga, P. Mukherjee, AJNR Am. J. Neuroradiol. **38**, 537–545 (2017)
17. N. Tyagi, M. Cloutier, K. Zakian, J.O. Deasy, M. Hunt, A. Rimner, J. Appl. Clin. Med. Phys. **20**, 284–292 (2019)
18. R. Matsuya, M. Kuroda, Y. Matsumoto, H. Kato, H. Matsuzaki, J. Asaumi, J. Murakami, K. Katashima, M. Ashida, T. Sasaki, T. Sei, K. Himei, K. Katsui, N. Katayama, M. Takemoto, S. Kanazawa, S. Mimura, S. Oono, T. Kitayama, K. Tahara, K. Inamura, Int. J. Oncol. **35**, 893–900 (2009)
19. I. Delakis, E.M. Moore, M.O. Leach, J.P. De Wilde, Phys. Med. Biol. **49**, 1409–1422 (2004)
20. H.J. Laubach, P.M. Jakob, K.O. Loevblad, A.E. Baird, M.P. Bovo, R.R. Edelman, S. Warach, J. Magn. Reson. Imaging **8**, 1349–1354 (1998)

21. G. Kalaitzakis, T. Boursianis, G. Gourzoulidis, S. Gourtsoyianni, G. Lymperopoulou, K. Marias, A. Karantanas, T.G. Maris, Phys. Med. **73**, 179–189 (2020)
22. T.-Q. Li, D.-H. Kim, M.E. Moseley, J. Magn. Reson. Imaging **21**, 468–475 (2005)
23. J.G. Hirsch, M. Bock, M. Essig, L.R. Schad, Magn. Reson. Imaging **17**, 705–716 (1999)
24. S. Gatidis, H. Schmidt, P. Martirosian, N.F. Schwenzer, Magn. Reson. Med. **72**, 459–463 (2014)
25. N.P. Jerome, M.V. Papoutsaki, M.R. Orton, H.G. Parkes, J.M. Winfield, M.A. Boss, M.O. Leach, N.M. de Souza, D.J. Collins, Med. Phys. **43**, 2998–3007 (2016)
26. P. Pullens, P. Bladt, J. Sijbers, A.I. Maas, P.M. Parizel, Med. Phys. **44**, 1063–1070 (2017)
27. O. Ashikyan, M. Chalian, D. Moore, Y. Xi, P. Pezeshk, A. Chhabra, Skelet. Radiol. **48**, 1765–1773 (2019)
28. D.C. Sullivan, N.A. Obuchowski, L.G. Kessler, D.L. Raunig, C. Gatsonis, E.P. Huang, M. Kondratovich, L.M. McShane, A.P. Reeves, D.P. Barboriak, A.R. Guimaraes, R.L. Wahl, Radiology **277**, 813–825 (2015)

Authors and Affiliations

Eisuke Sato[1] [ORCID] **· Kei Fukuzawa[2] · Hiroyuki Takashima[3] · Yuya Yamatani[4] · Yasuo Takatsu[5] · Junichi Hata[6] · Keigo Hikishima[7] · Kenta Miwa[8]**

Kei Fukuzawa
sappukei85157@gmail.com

Hiroyuki Takashima
takashima@sapmed.ac.jp

Yuya Yamatani
y-yama@naramed-u.ac.jp

Yasuo Takatsu
ytaka2.blue5@gmail.com

Junichi Hata
j.hata@jikei.ac.jp

Keigo Hikishima
k-hikishima@aist.go.jp

Kenta Miwa
kenta5710@gmail.com

[1] Department of Radiological Technology, Faculty of Health Science, Juntendo University, 3-2-12 Hongo, Bunkyo-ku, Tokyo 113-0033, Japan

[2] Department of Radiological Technology, Toranomon Hospital, Tokyo, Japan

[3] Division of Radiology and Nuclear Medicine, Sapporo Medical University Hospital, Sapporo, Japan

[4] Division of Central Radiology, Nara Medical University Hospital, Nara, Japan

[5] Department of Radiological Technology, Faculty of Health and Welfare, Tokushima Bunri University, Kagawa, Japan

[6] Division of Regenerative Medicine, Jikei University School of Medicine, Tokyo, Japan

[7] Medical Devices Research Group, Health and Medical Research Institute, National Institute of Advanced Industrial Science and Technology (AIST), Tsukuba, Japan

[8] Department of Radiological Sciences, School of Health Science, International University of Health and Welfare, Tochigi, Japan